AMERICAN SOCIETY FOR MICROBIOLOGY | Journal of Virology®

PATHOGENESIS AND IMMUNITY

Selective Interferon Responses of Intestinal Epithelial Cells Minimize Tumor Necrosis Factor Alpha Cytotoxicity

Jacob A. Van Winkle,[a] David A. Constant,[a] Lena Li,[a] Timothy J. Nice[a]

[a]Department of Molecular Microbiology and Immunology, Oregon Health & Science University, Portland, Oregon, USA

ABSTRACT Interferon (IFN) family cytokines stimulate genes (interferon-stimulated genes [ISGs]) that are integral to antiviral host defense. Type I IFNs act systemically, whereas type III IFNs act preferentially at epithelial barriers. Among barrier cells, intestinal epithelial cells (IECs) are particularly dependent on type III IFN for the control and clearance of virus infection, but the physiological basis of this selective IFN response is not well understood. Here, we confirm that type III IFN treatment elicits robust and uniform ISG expression in neonatal mouse IECs and inhibits the replication of IEC-tropic rotavirus. In contrast, type I IFN elicits a marginal ISG response in neonatal mouse IECs and does not inhibit rotavirus replication. *In vitro* treatment of IEC organoids with type III IFN results in ISG expression that mirrors the *in vivo* type III IFN response. However, IEC organoids have increased expression of the type I IFN receptor relative to neonate IECs, and the response of IEC organoids to type I IFN is strikingly increased in magnitude and scope relative to type III IFN. The expanded type I IFN-specific response includes proapoptotic genes and potentiates toxicity triggered by tumor necrosis factor alpha (TNF-α). The ISGs stimulated in common by type I and III IFNs have strong interferon-stimulated response element (ISRE) promoter motifs, whereas the expanded set of type I IFN-specific ISGs, including proapoptotic genes, have weak ISRE motifs. Thus, the preferential responsiveness of IECs to type III IFN *in vivo* enables selective ISG expression during infection that confers antiviral protection but minimizes disruption of intestinal homeostasis.

IMPORTANCE Enteric viral infections are a major cause of gastroenteritis worldwide and have the potential to trigger or exacerbate intestinal inflammatory diseases. Prior studies have identified specialized innate immune responses that are active in the intestinal epithelium following viral infection, but our understanding of the benefits of such an epithelium-specific response is incomplete. Here, we show that the intestinal epithelial antiviral response is programmed to enable protection while minimizing epithelial cytotoxicity that can often accompany an inflammatory response. Our findings offer new insight into the benefits of a tailored innate immune response at the intestinal barrier and suggest how dysregulation of this response could promote inflammatory disease.

KEYWORDS apoptosis, enteric viruses, epithelial cells, inflammation, interferons, intestinal immunity

Interferon (IFN) family cytokines provide antiviral defense through stimulation of a broad transcriptional response that includes direct-acting antiviral genes (1, 2). Members of the IFN family are divided into three types based on receptor usage: multiple type I IFN genes (many IFN-αs, IFN-β, and others [here IFN-α/β]), a single type II IFN gene (IFN-γ), and multiple type III IFN genes (up to four IFN-λs) (3, 4). IFN-α/β and IFN-λ are produced upon the detection of viral nucleic acids and are primary components of the early response to infection. The heterodimeric receptor for IFN-α/β (IFNAR) is expressed by most cell types, but the distinct heterodimeric receptor for IFN-λ (IFNLR)

Citation Van Winkle JA, Constant DA, Li L, Nice TJ. 2020. Selective interferon responses of intestinal epithelial cells minimize tumor necrosis factor alpha cytotoxicity. J Virol 94: e00603-20. https://doi.org/10.1128/JVI.00603-20.

Editor Julie K. Pfeiffer, University of Texas Southwestern Medical Center

Address correspondence to Timothy J. Nice, nice@ohsu.edu.

Received 2 April 2020
Accepted 17 August 2020
Accepted manuscript posted online 26 August 2020
Published 14 October 2020

is preferentially expressed by neutrophils and epithelial cells (4–6). Prior studies from us and others in mouse models of gastrointestinal virus infection have used receptor-deficient animals to show that IFN-λ is particularly important for the protection of intestinal epithelial cells (IECs) (7–10). Additional mouse studies suggest that IECs require IFN-λ for antiviral protection because they are less responsive to IFN-α/β than other epithelial cell types (7, 11, 12), which may result from downregulated IFNAR expression *in vivo* (7, 12). However, the physiological benefit of this preferential IEC responsiveness to IFN-λ has remained unclear.

The activation of IFNAR or IFNLR results in the phosphorylation of signal transducer and activator of transcription (STAT) transcription factors and the upregulation of IFN-stimulated genes (ISGs). More specifically, STAT1 and STAT2 are phosphorylated, bind interferon response factor 9 (IRF9), and form a heterotrimeric complex called interferon-stimulated gene factor 3 (ISGF-3). ISGF-3 translocates to the nucleus and binds interferon-stimulated response element (ISRE) motifs in ISG promoters (1, 13, 14). Additionally, STAT1 homodimers, other STAT family members, and noncanonical factors also play a role in the transcription of some ISGs (15, 16). Prior comparisons of ISG induction by IFN-λ or IFN-α/β in cultured hepatocytes revealed largely overlapping responses consisting of canonical antiviral ISGs (17–22). However, other in-depth studies of neutrophils and hepatocytes have indicated that IFN-α/β is generally more potent than IFN-λ and results in greater chemokine and cytokine production (23–27). Additionally, studies of IECs cultured *in vitro* as three-dimensional (3D) organoids have found that they are highly responsive to IFN-α/β, unlike IECs *in vivo* (28–33). Thus, the physiological basis of the preferential IEC responsiveness to IFN-λ *in vivo* remains unclear.

Here, we directly and quantitatively compare the IEC responses to IFN-β and IFN-λ *in vivo* and *in vitro*. We find that the *in vivo* IEC response to IFN-β is minimal and does not inhibit the replication of IEC-tropic rotavirus. In contrast, *in vitro* IFN-β treatment of IEC organoids elicits hundreds of ISGs, including proapoptotic genes, and potently blocks rotavirus infection. *In vitro* and *in vivo*, IECs are equally responsive to IFN-λ and upregulate known antiviral genes but not proapoptotic genes. Consistent with differing proapoptotic gene expression, we show that cytotoxicity triggered by tumor necrosis factor alpha (TNF-α) is increased in IEC organoids pretreated with IFN-β relative to IFN-λ. Finally, bioinformatic scoring of promoter motifs indicates that IFN-β-specific ISGs, including proapoptotic genes, have low-scoring, weak ISREs. Antiviral ISGs stimulated in common by IFN-λ and IFN-β have high-scoring, strong ISREs. Together, these findings suggest that the preferential responsiveness of IECs to IFN-λ *in vivo* ensures that antiviral ISGs are minimally accompanied by proapoptotic genes to promote epithelial homeostasis during clearance of enteric infection.

RESULTS

IECs in the neonatal intestine are minimally responsive to IFN-β. To extend our understanding of the transcriptional response to IFN in the intestine, we performed ISG *in situ* hybridization on intestinal tissues following IFN treatment *in vivo*. We injected phosphate-buffered saline (PBS), IFN-β, or IFN-λ3 into 7-day-old neonatal mice, which have low baseline ISG expression levels, and detected transcripts for a canonical ISG (*Usp18*) 4 h later. IFN-λ stimulated a robust increase in expression within the epithelial layer, with no visible stimulation of cells in the underlying lamina propria tissue (Fig. 1A). In contrast, IFN-β injection resulted in a modest increase of *Usp18* in dispersed cells of the epithelium and lamina propria (Fig. 1A).

To more quantitatively compare transcript abundances in IECs and intraepithelial hematopoietic cells, we sorted EpCAM-positive/CD45-negative epithelial ($EpCAM^+$) and CD45-positive/EpCAM-negative hematopoietic ($CD45^+$) cells from the dissociated epithelium by fluorescence-activated cell sorting (FACS). Consistent with the *in situ* hybridization results, quantitative PCR (qPCR) analysis showed that *Usp18* was stimulated more than 20-fold in $EpCAM^+$ cells following IFN-λ injection but less than 2-fold following IFN-β injection (Fig. 1B). Conversely, *Usp18* was stimulated less than 2-fold in

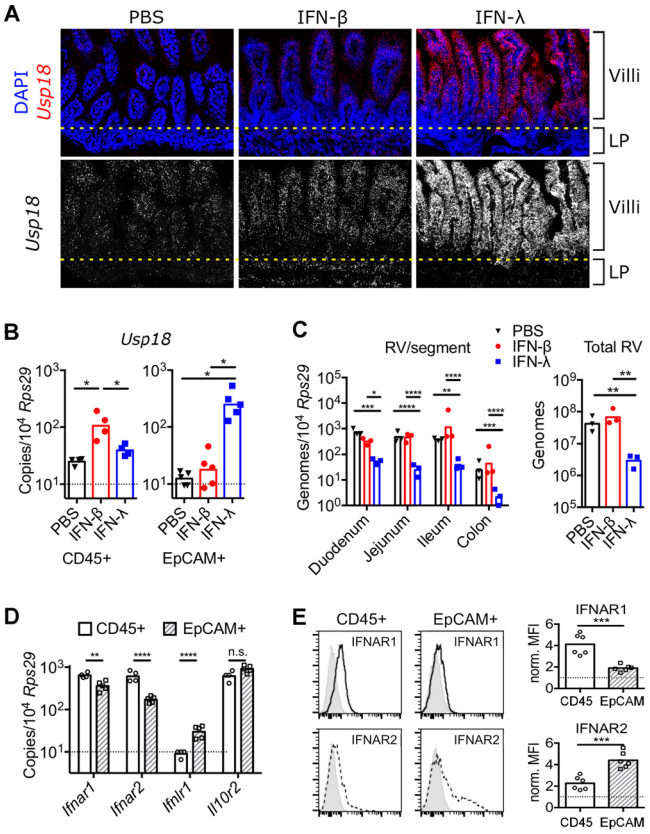

FIG 1 IECs in the neonatal intestine are minimally responsive to IFN-β. Neonatal mice were injected with either IFN-β or IFN-λ3 for 4 h. (A) Small intestinal tissue was isolated and stained with DAPI and *Usp18* antisense probes. The dashed line indicates the approximate boundary between villi and the lamina propria (LP). (B) *Usp18* abundance in sorted IECs (EpCAM positive/CD45 negative) and hematopoietic cells (CD45 positive/EpCAM negative) was determined by qPCR. (C) Mice were inoculated with rotavirus (RV), and viral genomes were quantitated in intestines 20 h later. (D) Comparison of IFN receptor gene abundances by qPCR in sorted EpCAM$^+$ IECs and CD45$^+$ hematopoietic cells. (E) Flow cytometry staining of IFNAR1 and IFNAR2 on EpCAM$^+$ IECs and CD45$^+$ hematopoietic cells. Gray histograms are control stains (no IFNAR antibody), and bar graphs show geometric mean fluorescence intensities (MFI) of IFNAR fluorescence normalized to the control for each replicate. Data are combined from at least two experiments with a total of three to five mice under each experimental condition; data points indicate individual animals, with bars indicating the means. Significance was determined by one-way or two-way analysis of variance (ANOVA) (B to D) or a *t* test (E). *, $P < 0.05$; **, $P < 0.01$; ***, $P < 0.001$; ****, $P < 0.0001$; n.s., not significant.

intraepithelial CD45$^+$ cells following IFN-λ injection but was stimulated 5-fold following IFN-β injection (Fig. 1B).

To determine whether *Usp18* transcripts were indicative of a broader ISG program that conferred antiviral protection to IECs, we challenged neonatal mice treated as described above with IEC-tropic murine rotavirus and quantitated viral genomes in the intestine 20 h later. IFN-λ injection resulted in 3- to 10-fold-lower numbers of viral genomes than PBS injection, but IFN-β injection provided no significant protection (Fig. 1C). These data align with previous reports of the preferential IEC response to IFN-λ in adult mice and suggest that hyporesponsiveness of IECs to IFN-α/β *in vivo* arises in early neonatal life.

To determine if IFN receptor gene expression correlated with responsiveness to cognate ligands, we performed qPCR for IFN receptor gene components in CD45$^+$ and EpCAM$^+$ cells sorted from neonatal intestines (Fig. 1B). Levels of transcripts encoding the IFNAR heterodimer (*Ifnar1* and *Ifnar2*) were relatively high in all cells but were 2-fold lower in EpCAM$^+$ IECs than in IFN-β-responsive CD45$^+$ cells (Fig. 1D). Transcripts for the specific subunit of the IFNLR heterodimer (*Ifnlr1*) were significantly more abundant in IFN-λ-responsive IECs than in CD45$^+$ intraepithelial cells but were less abundant overall

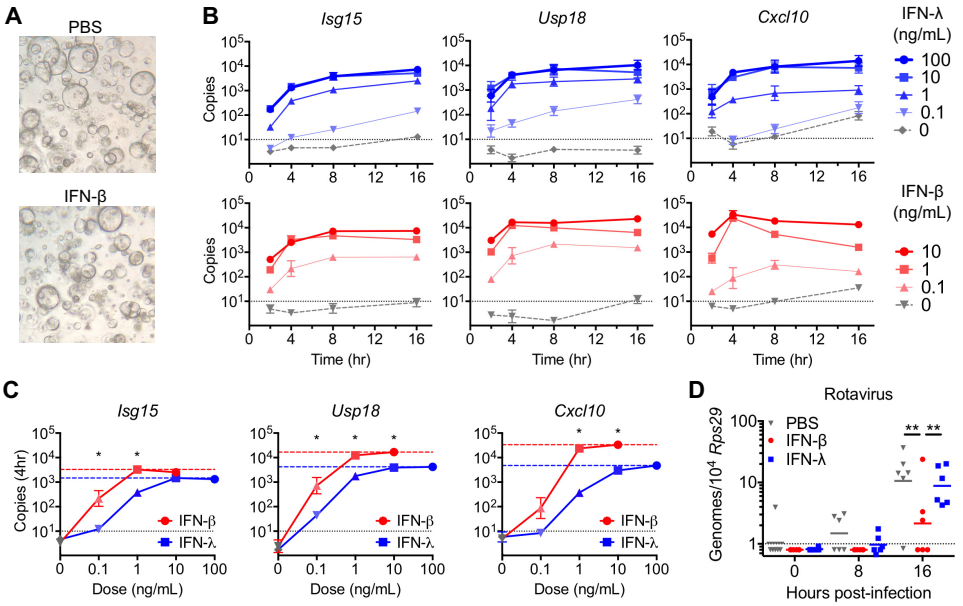

FIG 2 IEC organoids are dually responsive to IFN-β and IFN-λ. (A) Representative images of IEC organoids. (B) IEC organoids were treated with the indicated concentrations of recombinant IFN-β or IFN-λ2 for the indicated times, and RNA was isolated for the quantitation of *Isg15*, *Usp18*, and *Cxcl10* transcripts by qPCR. The dotted line indicates the limit of detection. (C) Transcript abundances of the indicated genes 4 h after IFN treatment across the range of IFN doses tested. Dashed lines indicate maximal responses for IFN-β or IFN-λ. (D) IEC organoids pretreated with PBS, IFN-β, or IFN-λ3 for 8 h were infected with rotavirus. Viral genomes were quantified at the indicated times postinfection. Data are from two (B and C) or three (D) experiments with duplicate treatment/infection wells; error bars show standard errors of the means (SEM). Statistical significance was determined by a *t* test (C) or one-way ANOVA (D). *, $P < 0.05$; **, $P < 0.01$.

than IFNAR gene transcripts. The transcript abundances of the other IFNLR1 subunit (*Il10rb*) were not significantly different between these cell types.

IFNAR abundance at the cell surface is regulated by both transcriptional and posttranscriptional mechanisms (34, 35). Therefore, we compared the surface expression levels of IFNAR1 and IFNAR2 subunits on CD45$^+$ and EpCAM$^+$ intestinal cells by flow cytometry. Staining for IFNAR1 was 4-fold above the background for CD45$^+$ cells and less than 2-fold above the background for EpCAM$^+$ cells; staining for IFNAR2 was 2-fold above the background for CD45$^+$ cells and 4-fold above the background for EpCAM$^+$ cells (Fig. 1E). Thus, the IFNAR1/IFNAR2 ratio is low on IECs relative to CD45$^+$ cells. These data suggest that the relatively low expression level of IFNAR1 on IECs of the neonatal intestine underlies IEC hyporesponsiveness to IFN-β *in vivo*, consistent with prior studies of IFNAR1 staining in adult mice (12).

IEC organoids are dually responsive to IFN-β and IFN-λ. To determine whether IFN-α/β hyporesponsiveness was intrinsic to IECs, we generated *in vitro* IEC organoids from isolated epithelial stem cells (Fig. 2A). We stimulated these IEC organoids with 0, 0.1, 1, 10, or 100 ng/ml of mouse IFN-β or IFN-λ2 for 2, 4, 8, or 16 h and quantitated the abundances of three canonical ISGs (*Isg15*, *Usp18*, and *Cxcl10*). The abundances of all three ISGs were increased by IFN-β and IFN-λ2 treatments, with maximal upregulation of between 100- and 1,000-fold (Fig. 2B). The expression kinetics were similar for all three ISGs following IFN-λ stimulation, with maximal upregulation at 4 to 8 h posttreatment and sustained expression at 16 h. Similar expression kinetics were observed for *Isg15* and *Usp18* following IFN-β stimulation. However, at the highest doses of IFN-β, *Cxcl10* reached a peak of induction at 4 h and decreased thereafter (Fig. 2B). Comparison of the dose responses for IFN-β or IFN-λ at 4 h posttreatment indicated that early ISG upregulation was between 2- and 10-fold greater for IFN-β than for IFN-λ (Fig. 2C). These data indicate that IEC organoids upregulate canonical ISGs in response to IFN-β and IFN-λ, with minimal differences in expression kinetics but a higher maximum

response to IFN-β. Therefore, the IFN-α/β hyporesponsiveness observed *in vivo* is not an intrinsic property of IECs.

To confirm that the above-described ISG expression was indicative of the overall antiviral program stimulated by IFN treatments, we challenged IEC organoids with murine rotavirus and quantitated viral genomes 0, 8, and 16 h later. IFN-λ treatment resulted in modest reductions in viral genomes relative to PBS treatment, but IFN-β treatment resulted in a 3- to 10-fold reduction in viral genomes (Fig. 2D). Therefore, IFN-β stimulates a stronger antiviral response than IFN-λ in cultured IEC organoids. These data indicate that the antiviral ISG response of IECs *in vivo* is regulated by factors not recapitulated in organoid culture.

Global ISG expression in response to IFN-β is suppressed *in vivo*. To more comprehensively compare the *in vivo* and *in vitro* IEC responses to IFN, we performed RNA sequencing (RNA-seq) on sorted EpCAM$^+$ cells from neonatal mice treated with PBS, IFN-β, or IFN-λ3 and compared the results to those for RNA-seq of IEC organoids treated with PBS, IFN-β, or IFN-λ2 for 4 h. Normalized read counts for *Usp18* were increased between 5- and 1,000-fold by IFN treatment, with a greater increase in IEC organoids by IFN-β treatment than by IFN-λ treatment and a greater increase in neonatal IECs by IFN-λ treatment than by IFN-β treatment (Fig. 3A). These differences are reflective of qPCR results from Fig. 1 and 2, validating the RNA-seq data set. Principal-component analysis (PCA) indicated that the primary component differentiating these samples (PC1) (95% of the variance) was their organoid or neonate origin and included differential expression of metabolism and cell cycle genes (Fig. 3B; see also Data Set S1 in the supplemental material). The secondary PCA component (PC2) (2% of the variance) separated IFN treatment groups from matched PBS controls (Fig. 3B).

We identified differentially expressed genes among IFN treatment groups relative to their corresponding PBS controls using liberal inclusion criteria (fold change of $>$1.5 and adjusted *P* value of $<$0.1). Few genes were downregulated by IFN treatments (Data Sets S2 and S3), consistent with the known transcriptional activation downstream of IFN receptors. The identification of ISGs in neonatal IECs revealed 210 IFN-λ-stimulated genes but only 64 IFN-β-stimulated genes (Fig. 3C and Data Set S2). Furthermore, all IFN-β-stimulated genes but one (63/64) were present among the 210 IFN-λ-stimulated genes (Fig. 3C). Therefore, the global early response of neonatal IECs to IFN-λ is substantially larger than that to IFN-β.

IEC organoids had a number of IFN-λ-stimulated genes (190) comparable to that of neonatal IECs (210), with the majority of genes (134) being present in both (Fig. 3D and E). However, in striking contrast to neonatal IECs, IEC organoids had a larger number (527) of IFN-β-stimulated genes (Fig. 3E). Among IEC organoid treatment groups, there were zero genes unique to IFN-λ, with all 190 IFN-λ-stimulated genes being present among the 527 IFN-β-stimulated genes (Fig. 3E and Data Set S3). Therefore, the early responses of IEC organoids to IFN-β and IFN-λ highly overlap, and IFN-λ-stimulated genes comprise a subset of IFN-β-stimulated genes.

To more comprehensively analyze the relationship between the IFN responses of neonate and organoid IECs, we normalized the $\log_2$-fold changes of all 527 organoid ISGs to matching PBS controls and plotted these changes on a heat map with hierarchical clustering (Fig. 3F). IFN-λ-stimulated neonate and organoid IECs clustered closer to each other than to other treatment groups, supporting the conclusion that IFN-λ responses are similar between neonate and organoid IECs. In contrast, IFN-β-stimulated neonatal IECs clustered closer to PBS controls than to other IFN treatment groups (Fig. 3F). These comparisons indicate that the *in vivo* hyporesponsiveness of IECs to IFN-α/β applies globally to all ISGs, whereas responsiveness to IFN-λ is a relatively stable IEC-intrinsic property.

To determine if the expression of IFNAR genes was correlated with the responsiveness of IECs to IFN-β, we compared the abundances of receptor genes in neonatal and organoid IECs. *Ifnar1*, *Ifnar2*, *Ifnlr1*, and *Il10rb* were not differentially expressed between

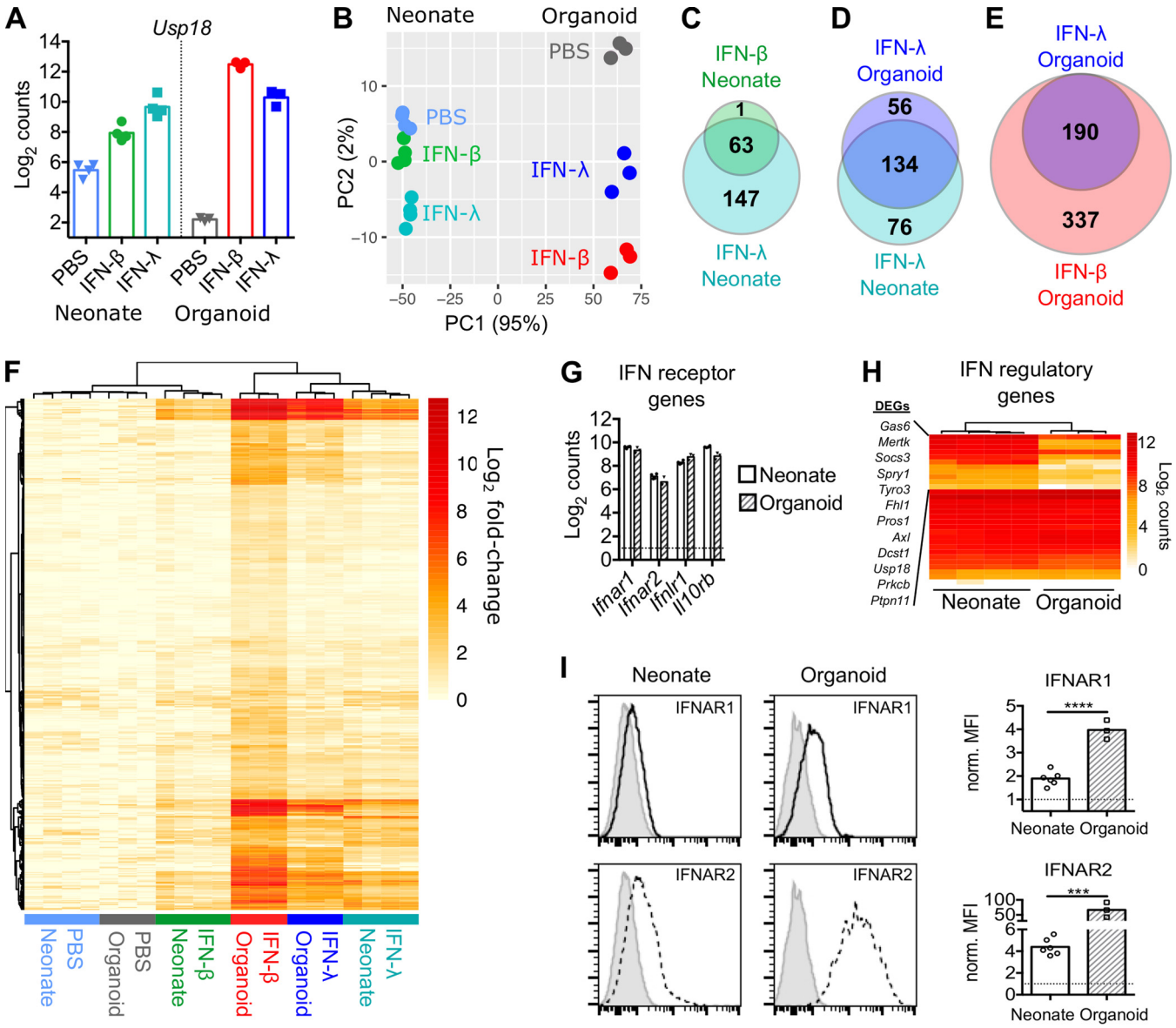

FIG 3 Global ISG expression in response to IFN-β is suppressed *in vivo*. IEC organoids or neonatal mice were treated for 4 h with PBS or IFN as described in the legends of Fig. 1 and 2, and isolated IECs were analyzed by RNA-seq. (A) Normalized read counts for *Usp18*. (B) PCA of the top 500 differentially expressed genes. (C to E) Venn diagrams showing the overlap in genes stimulated by the indicated IFN treatments relative to their matched PBS-treated controls. (F) Heat map comparing $\log_2$-fold changes of 527 ISGs among organoid and neonate IFN treatment groups relative to matched PBS controls. (G and H) Log_2 normalized counts of the indicated IFN receptor genes (G) and heat map of IFN regulatory genes (H) from PBS-treated neonate and organoid IECs. Differentially expressed genes (DEGs) listed in panel H are significantly different between neonate and organoid IECs (see Data Set S1 in the supplemental material). (I) Flow cytometry staining of IFNAR1 and IFNAR2 on neonate IECs (from Fig. 1E) and organoid IECs. Gray histograms are control stains (no IFNAR antibody), and bar graphs show geometric mean fluorescence intensities (MFI) of IFNAR fluorescence normalized to the controls. Data points represent results from replicate treatments (A, B, and G) or replicate experiments (I). Significance was determined by a *t* test (I). *, $P < 0.05$; **, $P < 0.01$.

these IEC types (Fig. 3G and Data Set S1). However, additional comparisons of 30 previously identified IFNAR regulatory genes curated from the literature (34–36) indicated that 11/30 of these genes were significantly more abundant in neonatal IECs than in organoid IECs, but only 1/30 was modestly more abundant in organoid IECs (Fig. 3H). The increased abundance of 11/30 known IFNAR-negative regulatory genes with minimal differences in IFNAR receptor genes suggested the potential for posttranscriptional suppression of IFNAR in neonatal IECs. Indeed, we found that surface staining of IFNAR1 and IFNAR2 was significantly increased on organoid IECs relative to neonatal IECs (Fig. 3I). Together, these data are consistent with a posttranscriptional mechanism of IEC hyporesponsiveness to IFN-β *in vivo*.

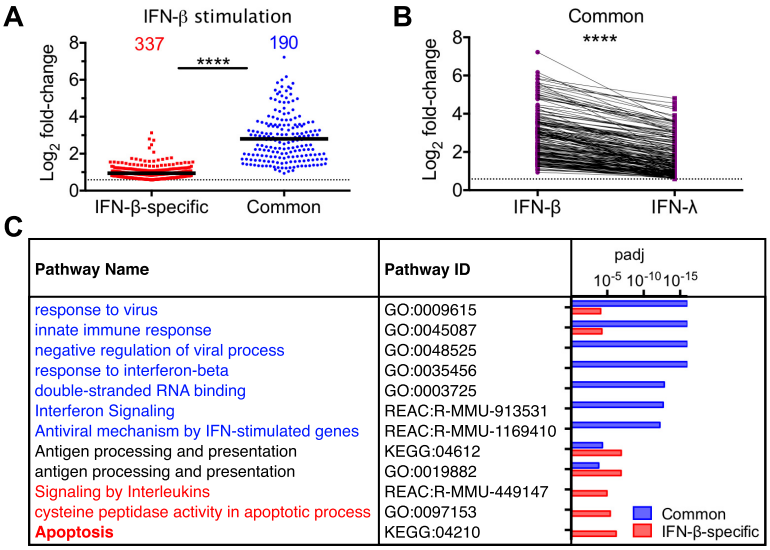

FIG 4 Common ISGs in IEC organoids are highly stimulated and consist of canonical antiviral genes. (A) Log_2-fold changes from RNA-seq of genes stimulated by IFN-β but not IFN-λ (337) (IFN-β specific) or genes stimulated by both IFN-β and IFN-λ (190) (common). (B) Comparison of log_2-fold changes for common ISGs following stimulation by IFN-β or IFN-λ. Lines indicate gene identity across treatment groups. (C) Selected pathways differentiating the indicated ISG categories. "padj" is the *P* value adjusted for multiple comparisons. For a complete list of pathways, see Data Set S4 in the supplemental material. Statistical significance was determined by a Mann-Whitney test. ****, $P < 0.0001$.

Apoptosis genes are among IFN-β-specific ISGs. The above-described data from neonatal mice, together with prior studies of adult mice, strongly suggest that hyporesponsiveness of IECs to IFN-α/β *in vivo* is physiologically advantageous. To gain insight into the potential advantages of selective IFN-λ responsiveness, we further analyzed the transcriptomes of IFN-β-responsive IEC organoids. The 337 "IFN-β-specific ISGs" of IEC organoids represented a subset of the overall IFN response that is not present *in vivo*, whereas the 190 genes stimulated by IFN-λ and IFN-β represented a "common ISG" module. Notably, the common ISGs were stimulated to a significantly greater extent by IFN-β treatment than the IFN-β-specific ISGs (Fig. 4A), and the 190 common ISGs were stimulated to a significantly greater extent by IFN-β than by IFN-λ treatment (Fig. 4B). Therefore, common ISGs consist almost entirely of the most highly responsive genes. To identify differential pathway associations, we compared the 337 IFN-β-specific ISGs with the 190 common ISGs using g:Profiler (37). Comparison of curated pathways from the gene ontology (GO), KEGG, and Reactome databases indicated that (i) common ISGs were more significantly associated with antiviral effector pathways, (ii) common ISGs and IFN-β-specific ISGs were similarly associated with antigen processing and presentation pathways, and (iii) IFN-β-specific ISGs were significantly associated with apoptosis pathways (Fig. 4C and Data Set S4). A heat map of all apoptosis pathway genes (KEGG:04210) confirmed that IFN-β-treated IEC organoids clustered separately from other treatment groups and controls (Fig. 5A). Specifically, IFN-β treatment of organoids uniquely stimulated 19/130 apoptosis pathway genes, including the proapoptotic genes *Bid*, *Bcl2l11*, and *Casp8* (Fig. 5A and B). Together, these analyses indicate that IFN-β and IFN-λ are similarly capable of eliciting antiviral effectors, but IFN-β uniquely stimulates the expression of apoptosis pathway genes.

Prior studies in other cell types have indicated that inflammatory cytokines are a gene set that distinguishes IFN-α/β from IFN-λ (23, 25). To determine whether these genes were also differentially regulated in our IEC organoid studies, we performed a focused analysis of 37 inflammatory cytokines, including interleukin-6 (IL-6), IL-1β, and TNF-α, shown by Galani et al. to be differentially regulated in neutrophils (25). Unlike neutrophils, the majority of these inflammatory cytokines were not stimulated in IEC organoids, with the notable exception of the proinflammatory chemokine *Cxcl10*

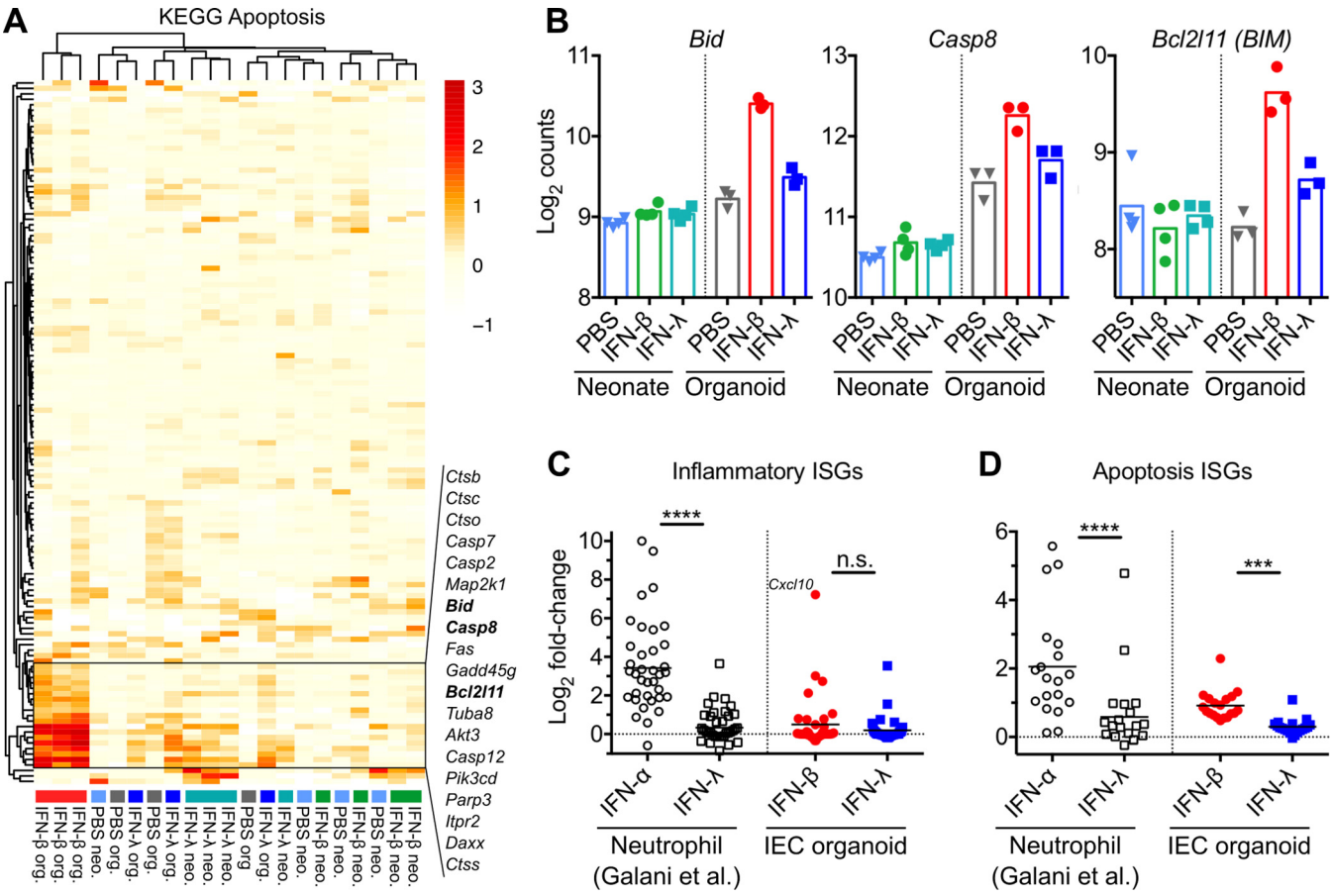

FIG 5 IFN-β-specific ISGs include apoptosis pathway genes. (A) Heat map comparing $\log_2$-fold changes of all KEGG apoptosis pathway genes among organoid and neonate IFN treatment groups relative to their corresponding PBS controls. Names are shown for the cluster of "apoptosis ISGs" stimulated by IFN-β treatment of organoids. (B) Normalized RNA-seq counts for three apoptosis ISGs. (C and D) $\log_2$-fold changes of inflammatory ISGs (C) or apoptosis ISGs (D) from IFN-treated neutrophils (25) (open circles, IFN-α; open squares, IFN-λ) or IEC organoids (filled circles, IFN-β; filled squares, IFN-λ) relative to their corresponding PBS controls. Statistical significance was determined by a Kruskal-Wallis test. ***, $P < 0.001$; ****, $P < 0.0001$; n.s., not significant ($P > 0.05$).

(Fig. 5C and Data Set S5). This suggests that neutrophils and IECs differ in their capacity for ISG expression. To determine whether this difference extended to the set of IFN-β-specific apoptosis ISGs identified here, we analyzed the expression of these genes in the RNA-seq data from the study by Galani et al. Similar to our results in IECs, neutrophils upregulated apoptosis pathway genes following treatment with IFN-α but not IFN-λ (Fig. 5D). These comparisons suggest that some IFN-α/β-specific ISGs (i.e., inflammatory cytokines) are cell type specific and that others (i.e., proapoptotic genes) are similar across cell types.

IFN-β potentiates TNF-α-triggered apoptosis. Among the apoptosis pathway genes identified in Fig. 5A, the *Bid* and *Casp8* gene products are integral effectors in the extrinsic apoptosis pathway triggered by the inflammatory cytokine TNF-α (38). To determine whether IFN-β treatment potentiates TNF-α-triggered apoptosis, we pretreated IEC organoid cultures with IFN-β, IFN-λ, or PBS followed by treatment with TNF-α and measured cell viability using the 3-(4,5-dimethyl-2-thiazolyl)-2,5-diphenyl-2H-tetrazolium bromide (MTT) assay (Fig. 6A). Treatment with TNF-α, IFN-β, or IFN-λ alone resulted in a minimal loss of IEC viability ($<$10%), suggesting that our IEC organoids are resistant to the cytotoxic effects of TNF-α at baseline. However, IFN-β treatment synergized with TNF-α and resulted in an average of a 30% loss in viability. In contrast, IFN-λ followed by TNF-α treatment resulted in significantly less (average, 18%) loss of viability (Fig. 6A). To confirm that death in these IEC organoid cultures was related to apoptosis, we examined cleaved (active) executioner caspase 3 (CC3) by

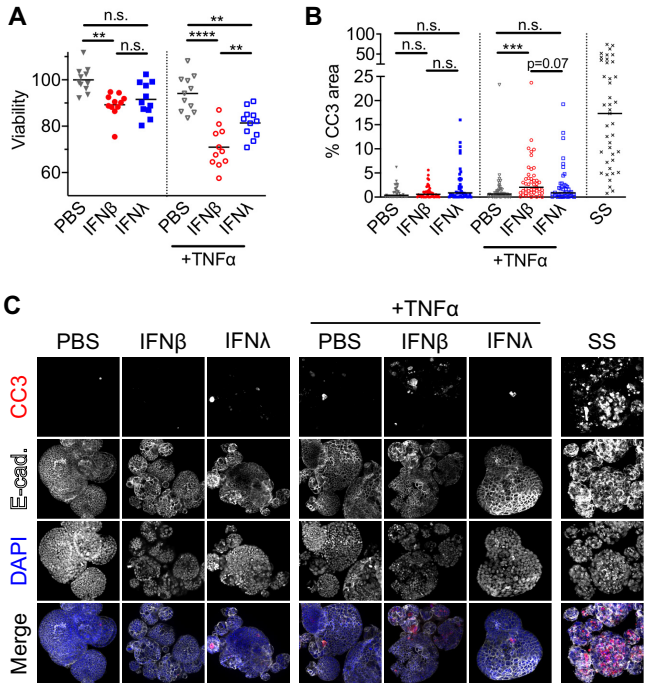

FIG 6 IFN-β potentiates TNF-α-triggered apoptosis. (A) MTT viability assay of IEC organoids treated with 10 ng/ml IFN-λ3, IFN-β, or PBS for 4 h followed by treatment with 100 ng/ml TNF-α for 20 h. (B and C) Cleaved caspase 3 (CC3) in IEC organoids was assessed by immunofluorescence following pretreatment with 10 ng/ml IFN-λ3, IFN-β, or PBS for 4 to 8 h and subsequent treatment with medium or 100 ng/ml TNF-α for 16 to 20 h. The positive apoptosis control, staurosporine (SS), was administered to PBS organoids for 16 to 20 h. Data are pooled from three independent experiments, with statistical significance determined by one-way ANOVA in panel A and by a Kruskal-Wallis test with Dunn's multiple comparisons in panel B. The solid line depicts the mean in panel A and the median in panel B. **, $P < 0.01$; ***, $P < 0.001$; ****, $P < 0.0001$; n.s., not significant ($P > 0.05$). E-cad., E-cadherin.

immunofluorescence. IFN-β treatment followed by TNF-α resulted in a significant increase in the percentage of cleaved caspase 3 in IEC organoids, whereas IFN-λ treatment did not (Fig. 6B and C). These data indicate that IFN-β stimulation results in greater sensitivity of IECs to TNF-α-triggered apoptosis and suggest that hyporesponsiveness of IECs to IFN-α/β *in vivo* favors epithelial viability.

The strength of the canonical ISRE differentiates ISG categories. To globally define distinguishing promoter motifs of common and IFN-β-specific ISG categories, we used the Hypergeometric Optimization of Motif EnRichment (HOMER) software package (39). We searched for motifs enriched in IFN-β-specific ISG promoters relative to a "background" of common ISG promoters or vice versa. This comparison resulted in no statistically significant promoter motifs that distinguished IFN-β-specific ISGs from common ISGs. However, a *de novo* motif was significantly enriched in common ISG promoters relative to IFN-β-specific ISG promoters (Fig. 7A). This common ISG motif was clustered near the transcription start sites (TSSs) of these genes, consistent with a direct role in initiating transcription (Fig. 7B). The *de novo* common ISG motif had a high degree of similarity to previously described ISRE and IRF motifs, suggesting that it reflected stronger canonical promoter motifs among common ISGs. Indeed, previously defined (canonical) ISRE and IRF motifs were present at a significantly higher frequency among common ISGs than among IFN-β-specific ISGs (Fig. 7A and Data Set S6). Further comparison of common ISGs and IFN-β-specific ISGs to a background of other genes within the mouse genome revealed that ISRE and IRF motifs were significantly enriched in both ISG sets, and a STAT1 motif was specifically enriched among common ISGs (Fig. 7A and B and Data Set S6). As a control for these comparisons, the GC-rich basal promoter motif of specificity protein 1 (Sp1) was found at a similar frequency near the TSSs of all gene categories (Fig. 7A and B).

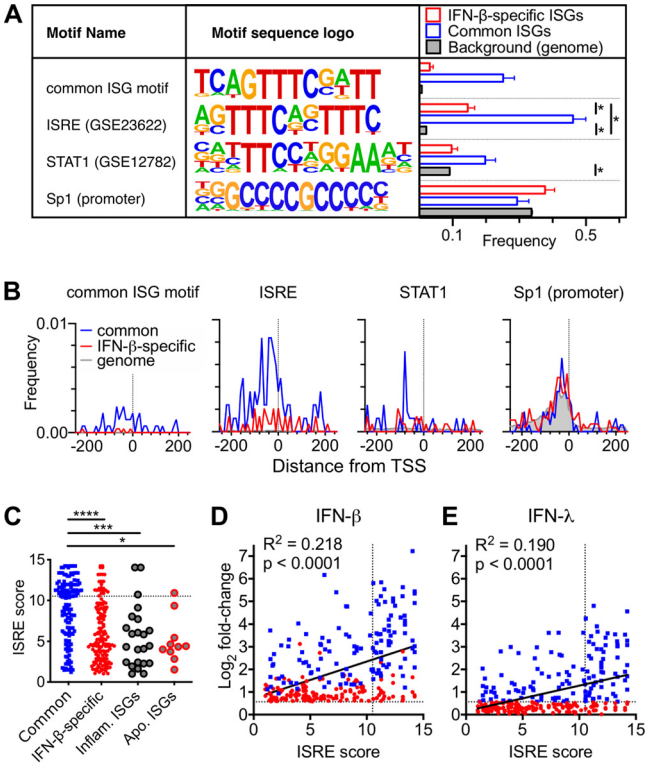

FIG 7 The strength of the canonical ISRE differentiates ISG categories. Motifs were identified in genomic sequences 500 bp upstream to 250 bp downstream of annotated transcriptional start sites (TSS) for gene sets. (A) Motif sequence logos for *de novo* common ISG motifs and known motifs from the HOMER database. The heights of bases are proportional to their preference at that position. The frequency graph depicts the proportion of genes in each category with at least one instance of the indicated motif scoring above the threshold, with * indicating a *q* value (false-discovery rate) of <0.05. (B) Histograms of motif locations relative to the TSS. (C) Comparison of ISRE (GEO series accession number GSE23622) motif scores among previously defined common, IFN-β-specific, apoptosis, and inflammatory ISGs. The dashed line indicates the threshold score from the analysis in panel A; the highest-scoring motif is shown for each gene with at least one motif score of >1. (D and E) Correlation of ISRE scores with $\log_2$-fold changes following treatment with IFN-β (D) or IFN-λ (E). The vertical dashed line indicates the threshold score from the analysis in panel A, and the horizontal dashed line indicates a 1.5-fold differential expression cutoff.

We were interested in determining how well the global analysis of IFN-β-specific ISG promoters reflected the properties of apoptosis ISGs and neutrophil inflammatory ISGs. Additionally, we sought to perform more quantitative motif comparisons beyond a simple presence/absence determination. So we determined the ISRE score for each gene, which is higher for promoter sequences that more closely match the ideal ISRE (Fig. 7A). ISRE motif scores were similarly low among apoptosis ISGs, inflammatory ISGs, and IFN-β-specific ISGs, all of which were significantly lower than those of common ISGs (Fig. 7C). These data indicate that promotor characteristics of IFN-β-specific ISGs as a whole are reflected in apoptosis and inflammatory gene subsets.

Prior studies in other cell types have indicated that IFN-λ stimulates less robust STAT1 phosphorylation and ISRE transactivation than IFN-α/β (18, 21). Consistent with these findings, we observed lower fold increases of common ISGs by IFN-λ than by IFN-β (Fig. 4B). To explore the relationship between ISRE scores and fold increases, we performed correlation analyses of these two variables for all ISGs. We observed a significant positive correlation between IFN-β-stimulated fold changes and ISRE scores, confirming the relevance of this promoter motif (Fig. 7D). The IFN-λ-stimulated fold change was also significantly correlated with the ISRE score but had a significantly shallower slope ($P = 0.0293$) (Fig. 7E). Together, these data indicated that ISGs with low-scoring ISRE motifs were less likely to be stimulated by IFN-λ and correspondingly more likely to be IFN-β specific.

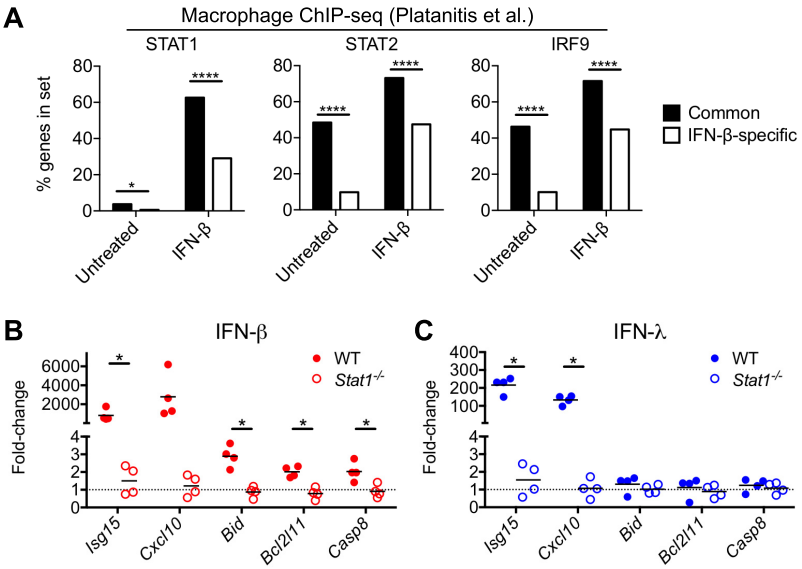

FIG 8 IFN-β-specific apoptosis ISGs are dependent on the canonical transcription factor STAT1. (A) Reanalysis of ChIP-seq data under GEO series accession number GSE115433 (52). Percentages of genes in common ISG and IFN-β-specific ISG sets that had significant ChIP-seq peaks for STAT1, STAT2, or IRF9 within 500 bp of the transcription start site are shown. Statistical significance was determined by a chi-square test of contingency tables of genes with or without peaks. *, $P < 0.05$; ****, $P < 0.0001$. (B and C) Quantitative PCR analysis of genes indicated on the *x* axis following treatment of WT or *Stat1*$^{-/-}$ IEC organoids with 10 ng/ml IFN-β (B) or IFN-λ3 (C) for 4 h, normalized to PBS-treated controls. Data are combined from four experiments, with * indicating a *P* value of <0.05 by one-way ANOVA.

IFN-β-specific apoptosis ISGs are dependent on the canonical transcription factor STAT1. The above-described bioinformatic analyses suggested that promoters of IFN-β-specific ISGs would be less effective in the recruitment of ISGF-3 components (STAT1, STAT2, and IRF9). To determine whether the binding of these canonical transcription factors to promoters of common ISGs differed from binding to promoters of IFN-β-specific ISGs, we reanalyzed a previously published data set (NCBI Gene Expression Omnibus [GEO] series accession number GSE115433) from the sequencing of DNA following chromatin immunoprecipitation (ChIP-seq) of STAT1, STAT2, and IRF9 from macrophages. According to these data, promoters of common ISGs were significantly more likely than promoters of IFN-β-specific ISGs to be precipitated with any ISGF-3 component from untreated or IFN-β-treated cells (Fig. 8A). These data are consistent with those from our bioinformatic analyses (Fig. 7) and suggest that lower-scoring ISRE motifs in promoters of IFN-β-specific ISGs result in less robust binding of STAT1, STAT2, and IRF9.

Despite the low-scoring ISRE motifs of IFN-β-specific ISGs, we hypothesized that their stimulation by IFN-β would remain dependent on the canonical usage of STAT1. To test this hypothesis, we generated IEC organoids from *Stat1*$^{-/-}$ mice that are unable to generate active STAT1 homodimers or heterotrimeric ISGF-3. We treated wild-type (WT) and *Stat1*$^{-/-}$ organoids with 10 ng/ml IFN-β or IFN-λ3 for 4 h followed by qPCR to measure the induction of common ISGs (*Isg15* and *Cxcl10*) and IFN-β-specific apoptosis ISGs (*Casp8*, *Bid*, and *Bcl2l11*). Common ISGs were induced >1,000-fold by IFN-β and >100-fold by IFN-λ in WT IECs. We confirmed that common ISGs were not induced by either IFN type in *Stat1*$^{-/-}$ IECs, consistent with an absolute requirement of STAT1 for their stimulation (Fig. 8A and B). Proapoptotic ISGs were induced 2- to 3-fold by IFN-β in WT IECs but were not induced by IFN-λ in WT IECs or by either treatment in *Stat1*$^{-/-}$ IECs (Fig. 8A and B). These data indicate that the IFN-β-specific ISGs *Casp8*, *Bid*, and *Bcl2l11* are dependent on canonical ISG transcription factors. Taken together, our findings support the conclusion that IFN-β-specific ISGs are largely distinguished by low-scoring ISRE promoter motifs rather than a unique noncanonical motif. In conclu-

sion, we propose a straightforward model in which a stronger transcriptional response downstream of IFN-β results in an expanded array of ISGs with low-scoring ISRE motifs. This expanded set of ISGs includes proapoptotic genes that have the potential to disrupt epithelial homeostasis and are therefore physiologically disadvantageous *in vivo*.

DISCUSSION

Here, we find that *in vivo* IECs are hyporesponsive to IFN-α/β beginning in early neonatal life (Fig. 1), thereby elevating the importance of IFN-λ in epithelial antiviral immunity. Prophylactic IFN-λ, but not IFN-β, reduces early replication of IEC-tropic mouse rotavirus, consistent with prior studies by Pott et al. (7). This ineffective IFN-β response of neonatal IECs was somewhat unanticipated based on a prior study by Lin et al., who found that IFN-α/β stimulated phospho-STAT1 in IECs of neonatal but not adult mice (11). Our transcriptomic comparison of ISG responses indicates that phospho-STAT1 may underlie a modest transcriptional response to IFN-β in neonatal IECs, but it is significantly diminished relative to the *in vivo* response of neonatal IECs to IFN-λ or the *in vitro* response of IEC organoids to IFN-β (Fig. 3). In fact, we find that IEC organoids expanded *in vitro* from intestinal stem cells are highly responsive to IFN-β, with robust ISG induction relative to IFN-λ (Fig. 2). This IFN response profile of mouse IEC organoids is consistent with recent human IEC organoid studies that found that IFN-α/β provides more potent antiviral protection from rotavirus (28, 29). We suggest that, similar to mouse IECs, human IECs in their natural context *in vivo* may become hyporesponsive to IFN-α/β.

Our studies of viral infection in mouse IEC organoids here together with prior studies in human IEC organoids by others present a paradox: IFN-λ is the dominant effector in mouse models of gastrointestinal virus infection, whereas IFN-α/β elicits superior antiviral defense *in vitro* (28). Our work here shows that IFN-β treatment of IEC organoids, in addition to stimulating significantly greater production of antiviral ISGs than IFN-λ, stimulates an expanded set of ISGs with low-scoring ISRE motifs (Fig. 7). This expanded ISG profile includes proapoptotic genes that potentiate TNF-α-triggered cytotoxicity (Fig. 6). These findings in IECs are reminiscent of recent studies in neutrophils that identified a set of inflammatory cytokine genes, including TNF-α, triggered by IFN-β but not IFN-λ (25). We find here that IECs are not capable of readily producing most of these inflammatory ISGs in response to IFN-β, emphasizing the importance of cell-lineage-specific studies (Fig. 5C). However, when considered in the context of the above-described neutrophil studies, our findings here suggest that a neutrophilic, inflamed intestine is a scenario in which IEC hyporesponsiveness to IFN-α/β would be particularly beneficial. If IECs were not hyporesponsive in this inflammatory scenario, IFN-α/β would synergistically elicit TNF-α production by neutrophils and potentiate TNF-α-triggered cytotoxicity of IECs. Indeed, such a synergistic response may explain observations of epithelial apoptosis in the IFN-α/β-responsive lung epithelium during influenza virus infection, where IFN-α but not IFN-λ treatment amplifies the apoptosis of lung epithelial cells (26). In addition to the less damaging ISG profile of IFN-λ, Broggi et al. showed that IFN-λ can actively suppress inflammatory responses of neutrophils by a posttranscriptional mechanism, providing further homeostatic benefits (27). Thus, the hyporesponsiveness of IECs to IFN-α/β *in vivo* may be moderately disadvantageous for antiviral protection but reduces the risk of inflammatory response amplification loops that result in epithelial damage.

Previous work suggested that apical trafficking of IFNAR and reduced *Ifnar1*/*Ifnar2* transcript expression are mechanisms for IEC hyporesponsive to IFN-α/β *in vivo* (7, 12). Our study supports a role for the posttranscriptional regulation of IFNAR1 and IFNAR2 in determining IEC responsiveness to IFN-α/β. IEC organoids have increased surface staining for both IFNAR subunits and reduced expression of several known negative regulators of IFNAR signaling. These mechanisms may relate to postnatal changes in intestinal exposure to nutrients and the microbiome, which elicit corresponding changes in IEC metabolism and immunity. Neil et al. recently showed

that when the microbiome is depleted from adult mice with antibiotics and the epithelium is exposed to damaging dextran sodium sulfate (DSS), an IFN-α/β response in IECs can promote the beneficial recruitment of IL-22-producing leukocytes (40, 41). This role of IFN-α/β in IECs suggests the following possibilities: (i) depletion of the microbiome together with epithelial damage could increase the IFN-α/β responsiveness of IECs, or (ii) under certain types of epithelial damage, the modest responsiveness of IECs to IFN-α/β *in vivo* may be beneficial. Further studies are needed to determine the effect of the microbiome and inflammatory triggers on the IFN-α/β responsiveness of IECs and to understand the signals that regulate IEC-intrinsic IFNAR responses *in vivo*. Our work here emphasizes the important pleiotropic roles of the IFN response and provides a physiological basis for regulating the ISG expression capacity of IECs to maintain intestinal homeostasis.

MATERIALS AND METHODS

Mice. C57BL/6J, BALB/c, and *Stat1*$^{-/-}$ (*Stat1*^{tm1Dlv}) mice were obtained from Jackson Laboratories and bred in specific-pathogen-free barrier facilities at Oregon Health & Science University (OHSU). Animal protocols were approved by the institutional animal care and use committee at Oregon Health & Science University (protocol number IP00000228) according to standards set forth in the Animal Welfare Act. A total of 0.2 μg IFN-β (catalog number 12405-1; PBL) or IFN-λ3 (catalog number 12820-1; PBL) was administered to 7-day-old neonatal mice via subcutaneous injection; an equal volume of a diluent (PBS) was administered to littermate control mice.

Rotavirus infection of mice. Mouse rotavirus strain EC was generously provided by Andrew Gewirtz (Georgia State University). Virus stocks were generated by inoculating 4- to 6-day-old neonatal BALB/c mice and collecting the entire gastrointestinal tract upon observation of diarrhea 4 to 7 days later. Intestines were subjected to a freeze-and-thaw cycle, suspended in PBS, homogenized in a bead beater using 1.0-mm zirconia-silica beads (BioSpec Products), clarified of debris, and aliquoted for storage at −70°C. The 50% shedding dose (SD_{50}) was determined by inoculation of 10-fold serial dilutions in adult C57BL/6J mice. For protection studies, 7-day-old neonatal mice were orally inoculated with 100 SD_{50}s, and intestines were isolated 20 h later for the quantitation of viral genomes by qPCR.

RNAscope. Swiss rolls of intestinal tissue were fixed in 10% neutral buffered formalin for 18 to 24 h and paraffin embedded. Tissue sections (5 μm) were cut and maintained at room temperature with a desiccant until processed. RNA *in situ* hybridization was performed using the RNAscope multiplex fluorescent v2 kit (Advanced Cell Diagnostics [ACDBio]) according to protocol guidelines. Staining with antisense probes for the detection of *Usp18* (catalog number 524651; ACDBio) was performed using ACDBio protocols and reagents. Slides were stained with 4′,6-diamidino-2-phenylindole (DAPI), mounted with ProLong Gold antifade reagent (Thermo Fisher), and imaged using the Zeiss ApoTome2 system on an Axio Imager, with a Zeiss AxioCam 506 camera.

Organoid culture. Primary organoid culture medium was advanced Dulbecco's modified Eagle's medium (DMEM)–F-12 medium (catalog number 12634010; Thermo Fisher) supplemented with 20% fetal bovine serum, 1× penicillin-streptomycin–L-glutamine, and 10 mM HEPES. Isolation and culture of primary mouse IEC organoids were performed essentially as described previously (42). Briefly, intestinal crypts were isolated by mechanical disruption, digestion with 2 mg/ml collagenase type I, and centrifugation. Isolated crypts were resuspended in 15 μl Matrigel (catalog number 354234; Corning) per well and plated in 24-well plates. Organoids were grown and maintained in 50% primary organoid culture medium mixed with 50% conditioned medium (CM) from L-WRN cells (ATCC CRL-3276), which contained Wnt3a, R-spondin3, and Noggin. A ROCK inhibitor (catalog number S1049; Selleck Chemicals) and a transforming growth factor β (TGF-β) inhibitor (catalog number S1067; Selleck Chemicals) were added to the culture medium to promote the survival of dissociated cells. The medium was replaced every 2 days. Every 3 days, or when organoids became dense, cells were disrupted with trypsin-EDTA and replated at ~30,000 cells/well. IFN-β (catalog number 12405-1; PBL), pegylated IFN-λ2 (Bristol-Meyers Squibb), IFN-λ3 (catalog number 12820-1; PBL), and TNF-α (catalog number 315-01A; Peprotech) were added to organoid cultures as indicated in the figure legends. For flow cytometry of organoid-derived IECs, organoids were first isolated from Matrigel by incubation in a cell recovery solution (catalog number 354253; Corning) at 4°C for 30 min, and IECs were then isolated from organoids by digestion with Accutase (catalog number AT-104; Innovative Cell Technologies) at 4°C for 30 min.

IEC organoid viability assays were adapted from methods described previously by Grabinger et al. (43). Organoids were seeded in 96-well plates at 500 to 1,000 cells per 5 μl Matrigel per well. Following cytokine treatment as indicated in the figure legends, MTT (catalog number MM5655; Sigma) was added to the cell culture medium at 0.5 mg/ml, and the culture was incubated at 37°C for 1 h. The medium was replaced with 100% dimethyl sulfoxide (DMSO), and the absorbance was measured at 570 nm on a BioTek plate reader. Background-subtracted optical density (OD) values were normalized to values for untreated organoid wells (100% viability) for each independent experiment.

Rotavirus infection of organoids. Primary mouse IEC organoids were dissociated to the single-cell level with trypsin-EDTA and seeded at ~25,000 cells/well. Organoids were maintained in 50% CM for 2 days, followed by 1 day of culture in 5% CM; the ROCK inhibitor and TGF-β inhibitor were supplemented to maintain the concentrations present in 50% CM. Cells were treated for 8 h with 10 ng/ml IFN-β (catalog number 12405-1; PBL), 10 ng/ml IFN-λ3 (catalog number 12820-1; PBL), or the PBS control.

Organoids were inoculated with 500 SD_{50}s of murine rotavirus EC in 5% CM by overlaying the inoculant, rocking at room temperature for 30 min, and washing with PBS three times. Infected cells were incubated in 5% CM until the indicated time points. Cells were lysed in ZR viral RNA buffer (Zymo Research), and viral genomes were detected by quantitative real-time PCR (RT-PCR).

Organoid immunofluorescence. Following stimulation, organoids were removed from Matrigel by rocking at 4°C in a cell recovery solution (Corning). Cells were stained by using methods adapted from previously described protocols (44). In short, cells were fixed in 3.7% paraformaldehyde, permeabilized in ice-cold 100% methanol, and blocked in a solution containing 5% normal goat serum, 5% bovine serum albumin, and 0.5% saponin in PBS. Cells were stained with mouse anti-E-cadherin (catalog number 610182; Becton, Dickinson), rabbit anti-cleaved caspase 3 (catalog number 9661S; Cell Signaling Technology), secondary goat anti-mouse Alexa Fluor 555, and goat anti-rabbit Alexa Fluor 647 (Thermo Fisher) in a solution containing 1% normal goat serum, 1% bovine serum albumin, and 0.5% saponin in PBS. IEC organoids were counterstained with DAPI, mounted with ProLong Gold antifade reagent (Thermo Fisher), and imaged using the Zeiss ApoTome2 system on an Axio Imager, with a Zeiss AxioCam 506 camera. The CC3-positive area was measured and normalized to the total area of the organoid surface using ImageJ.

Quantitative RT-PCR. RNA was isolated using RiboZol (Amresco) or the ZR viral RNA kit (Zymo Research). DNA contamination was removed using a DNA-free kit (Life Technologies). cDNA was generated with ImPromII reverse transcriptase (Promega). Quantitative PCR was performed using PerfeCTa qPCR FastMix II (QuantaBio) and primers and probes for the following targets: *Bid* (Integrated DNA Technologies [IDT] assay number Mm.PT.58.8829163), *Bcl2l11* (IDT assay number Mm.PT.58.12605058), *Casp8* (IDT assay number Mm.PT.58.41467226), *Isg15* (IDT assay number Mm.PT.58.41476392.g), *Usp18* (IDT assay number Mm.PT.58.28965870), *Cxcl10* (IDT assay number Mm.PT.58.28790444), *Rps29* (IDT assay number Mm.PT.58.21577577), and mouse rotavirus (primer 1, GTTCGTTGTGCCTCATTCG; primer 2, TCG GAACGTACTTCTGGAC; probe, AGGAATGCTTCAGCGCTG). The absolute copy number was determined by comparing threshold cycle (C_T) values to a standard curve generated using DNA of a known copy number encoding the target sequence. Samples are graphed as the absolute copy number of the indicated target divided by the absolute copy number of a housekeeping gene (*Rps29*). Samples with fewer than 1,000 copies of the housekeeping gene were excluded.

Cell isolation and flow cytometry. Epithelial fractions were prepared by nonenzymatic dissociation as previously described (45). Briefly, intestines of neonatal (7-day-old) mice were isolated, opened longitudinally, and incubated in stripping buffer (10% bovine calf serum, 15 mM HEPES, 5 mM EDTA, and 5 mM dithiothreitol [DTT] in PBS) with shaking for 20 min at 37°C. The dissociated cells were collected and stained for fluorescence-activated cell sorting (FACS). Cells were stained with Zombie Aqua viability dye (BioLegend), Fc receptor-blocking antibody (CD16/CD32; BioLegend), anti-EpCAM (clone G8.8; BioLegend), and anti-CD45 (clone 30-F11; BioLegend). For analysis of IFNAR expression, cells were additionally stained with anti-IFNAR1 (clone MAR1; BioLegend) or anti-IFNAR2 (polyclonal goat IgG; R&D Systems), and data were analyzed using FlowJo software (BD Biosciences). For the isolation of RNA, cells in the live gate were sorted as EpCAM-positive/CD45-negative IECs or EpCAM-negative/CD45-positive hematopoietic cells.

RNA sequencing. The quality of the RNA samples was assessed using the TapeStation system (Agilent), and mRNA sequencing libraries were prepared using the TruSeq RNA library prep kit (Illumina). Barcoded triplicate samples from IEC organoids (9 total) and quadruplicate samples from neonates (12 total) were separately prepared and pooled. Single-read sequencing was performed using the Illumina HiSeq 2500 platform through the Massively Parallel Sequencing Shared Resource at OHSU.

RNA-seq and ChIP-seq analyses. Adaptor-trimmed reads were mapped to the mouse genome (GRCm38) using the STAR aligner (46), and mapping quality was evaluated using RSeQC (47) and MultiQC (48). All samples had between 15 million and 30 million uniquely mapped reads with similar distributions across genomic features and uniform gene body coverage. Read counts per gene were determined using the featureCounts program (49), and differential expression analysis was performed using DEseq2, as described previously (50). PCA was performed on DEseq2 regularized logarithm (rlog)-transformed data. Heat maps were generated using $\log_2$-transformed data normalized to the mean of matched PBS control samples; heat map clustering is based on Euclidean distance.

ChIP-seq data from a study by Platanitis et al. were downloaded from the GEO (series accession number GSE115433), and narrowpeak files were analyzed using BEDOPS v.2.4.36 closest-features (51) to identify peaks within 500 bp of annotated transcription start sites associated with genes contained in the defined gene sets (common ISGs and IFN-β-specific ISGs). Genes were then classified as having either one or more ChIP-seq peaks associated with them or zero associated peaks.

Statistical analyses. Data were analyzed with GraphPad Prism software, with specified tests as noted in the figure legends.

Data availability. RNA sequencing data obtained in this study have been deposited in the NCBI Gene Expression Omnibus under GEO series accession number GSE142166.

SUPPLEMENTAL MATERIAL

Supplemental material is available online only.

SUPPLEMENTAL FILE 1, XLSX file, 1.5 MB.

SUPPLEMENTAL FILE 2, XLSX file, 0.1 MB.

SUPPLEMENTAL FILE 3, XLSX file, 0.1 MB.

SUPPLEMENTAL FILE 4, XLSX file, 0.7 MB.

SUPPLEMENTAL FILE 5, XLSX file, 0.5 MB.
SUPPLEMENTAL FILE 6, XLSX file, 0.1 MB.
SUPPLEMENTAL FILE 7, XLSX file, 0.1 MB.

ACKNOWLEDGMENTS

We thank the following OHSU core facilities for technical support: the Integrated Genomics Laboratory, the Advanced Light Microscopy Core, the Flow Cytometry Core, and the Histopathology Core.

T.J.N. was supported by NIH grant R01-AI130055 and by a faculty development award from the Sunlin and Priscilla Chou Foundation. J.A.V.W. was supported by NIH grants T32-GM071338 and T32-AI007472. D.A.C. was supported by NIH grant T32-AI007472. The funders had no role in study design, data collection and interpretation, or the decision to submit the work for publication.

Conceptualization, T.J.N.; Methodology, J.A.V.W., D.A.C., L.L., and T.J.N.; Investigation, J.A.V.W., D.A.C., L.L., and T.J.N.; Writing – Original Draft, T.J.N.; Writing – Review & Editing, J.A.V.W. and D.A.C.; Visualization, T.J.N.; Supervision, T.J.N.; Project Administration, L.L. and T.J.N.; Funding Acquisition, T.J.N.

We declare no competing interests.

REFERENCES

1. Sadler AJ, Williams BRG. 2008. Interferon-inducible antiviral effectors. Nat Rev Immunol 8:559–568. https://doi.org/10.1038/nri2314.
2. Schoggins JW, Rice CM. 2011. Interferon-stimulated genes and their antiviral effector functions. Curr Opin Virol 1:519–525. https://doi.org/10.1016/j.coviro.2011.10.008.
3. Mesev EV, LeDesma RA, Ploss A. 2019. Decoding type I and III interferon signalling during viral infection. Nat Microbiol 4:914–924. https://doi.org/10.1038/s41564-019-0421-x.
4. Lazear HM, Nice TJ, Diamond MS. 2015. Interferon-λ: immune functions at barrier surfaces and beyond. Immunity 43:15–28. https://doi.org/10.1016/j.immuni.2015.07.001.
5. Sommereyns C, Paul S, Staeheli P, Michiels T. 2008. IFN-lambda (IFN-lambda) is expressed in a tissue-dependent fashion and primarily acts on epithelial cells in vivo. PLoS Pathog 4:e1000017. https://doi.org/10.1371/journal.ppat.1000017.
6. Ye L, Schnepf D, Staeheli P. 2019. Interferon-λ orchestrates innate and adaptive mucosal immune responses. Nat Rev Immunol 19:614–625. https://doi.org/10.1038/s41577-019-0182-z.
7. Pott J, Mahlakõiv T, Mordstein M, Duerr CU, Michiels T, Stockinger S, Staeheli P, Hornef MW. 2011. IFN-lambda determines the intestinal epithelial antiviral host defense. Proc Natl Acad Sci U S A 108:7944–7949. https://doi.org/10.1073/pnas.1100552108.
8. Nice TJ, Baldridge MT, McCune BT, Norman JM, Lazear HM, Artyomov M, Diamond MS, Virgin HW. 2015. Interferon-λ cures persistent murine norovirus infection in the absence of adaptive immunity. Science 347:269–273. https://doi.org/10.1126/science.1258100.
9. Nice TJ, Robinson BA, Van Winkle JA. 2018. The role of interferon in persistent viral infection: insights from murine norovirus. Trends Microbiol 26:510–524. https://doi.org/10.1016/j.tim.2017.10.010.
10. Baldridge MT, Lee S, Brown JJ, McAllister N, Urbanek K, Dermody TS, Nice TJ, Virgin HW. 2017. Expression of Ifnlr1 on intestinal epithelial cells is critical to the antiviral effects of interferon lambda against norovirus and reovirus. J Virol 91:e02079-16. https://doi.org/10.1128/JVI.02079-16.
11. Lin J, Feng N, Sen A, Balan M, Tseng H, McElrath C, Smirnov S, Peng J, Yasukawa L, Durbin RK, Durbin JE, Greenberg HB, Kotenko SV. 2016. Distinct roles of type I and type III interferons in intestinal immunity to homologous and heterologous rotavirus infections. PLoS Pathog 12:e1005600. https://doi.org/10.1371/journal.ppat.1005600.
12. Mahlakõiv T, Hernandez P, Gronke K, Diefenbach A, Staeheli P. 2015. Leukocyte-derived IFN-α/β and epithelial IFN-λ constitute a compartmentalized mucosal defense system that restricts enteric virus infections. PLoS Pathog 11:e1004782. https://doi.org/10.1371/journal.ppat.1004782.
13. Kotenko SV, Gallagher G, Baurin VV, Lewis-Antes A, Shen M, Shah NK, Langer JA, Sheikh F, Dickensheets H, Donnelly RP. 2003. IFN-lambdas mediate antiviral protection through a distinct class II cytokine receptor complex. Nat Immunol 4:69–77. https://doi.org/10.1038/ni875.
14. Sheppard P, Kindsvogel W, Xu W, Henderson K, Schlutsmeyer S, Whitmore TE, Kuestner R, Garrigues U, Birks C, Roraback J, Ostrander C, Dong D, Shin J, Presnell S, Fox B, Haldeman B, Cooper E, Taft D, Gilbert T, Grant FJ, Tackett M, Krivan W, McKnight G, Clegg C, Foster D, Klucher KM. 2003. IL-28, IL-29 and their class II cytokine receptor IL-28R. Nat Immunol 4:63–68. https://doi.org/10.1038/ni873.
15. Au-Yeung N, Mandhana R, Horvath CM. 2013. Transcriptional regulation by STAT1 and STAT2 in the interferon JAK-STAT pathway. JAKSTAT 2:e23931. https://doi.org/10.4161/jkst.23931.
16. Ivashkiv LB, Donlin LT. 2014. Regulation of type I interferon responses. Nat Rev Immunol 14:36–49. https://doi.org/10.1038/nri3581.
17. Kohli A, Zhang X, Yang J, Russell RS, Donnelly RP, Sheikh F, Sherman A, Young H, Imamichi T, Lempicki RA, Masur H, Kottilil S. 2012. Distinct and overlapping genomic profiles and antiviral effects of interferon-λ and -α on HCV-infected and noninfected hepatoma cells. J Viral Hepat 19:843–853. https://doi.org/10.1111/j.1365-2893.2012.01610.x.
18. Marcello T, Grakoui A, Barba-Spaeth G, Machlin ES, Kotenko SV, MacDonald MR, Rice CM. 2006. Interferons alpha and lambda inhibit hepatitis C virus replication with distinct signal transduction and gene regulation kinetics. Gastroenterology 131:1887–1898. https://doi.org/10.1053/j.gastro.2006.09.052.
19. Zhou Z, Hamming OJ, Ank N, Paludan SR, Nielsen AL, Hartmann R. 2007. Type III interferon (IFN) induces a type I IFN-like response in a restricted subset of cells through signaling pathways involving both the Jak-STAT pathway and the mitogen-activated protein kinases. J Virol 81:7749–7758. https://doi.org/10.1128/JVI.02438-06.
20. Bolen CR, Ding S, Robek MD, Kleinstein SH. 2014. Dynamic expression profiling of type I and type III interferon-stimulated hepatocytes reveals a stable hierarchy of gene expression. Hepatology 59:1262–1272. https://doi.org/10.1002/hep.26657.
21. Doyle SE, Schreckhise H, Khuu-Duong K, Henderson K, Rosler R, Storey H, Yao L, Liu H, Barahmand-Pour F, Sivakumar P, Chan C, Birks C, Foster D, Clegg CH, Wietzke-Braun P, Mihm S, Klucher KM. 2006. Interleukin-29 uses a type 1 interferon-like program to promote antiviral responses in human hepatocytes. Hepatology 44:896–906. https://doi.org/10.1002/hep.21312.
22. Jilg N, Lin W, Hong J, Schaefer EA, Wolski D, Meixong J, Goto K, Brisac C, Chusri P, Fusco DN, Chevaliez S, Luther J, Kumthip K, Urban TJ, Peng LF, Lauer GM, Chung RT. 2014. Kinetic differences in the induction of interferon stimulated genes by interferon-α and interleukin 28B are altered by infection with hepatitis C virus. Hepatology 59:1250–1261. https://doi.org/10.1002/hep.26653.
23. Forero A, Ozarkar S, Li H, Lee CH, Hemann EA, Nadjsombati MS, Hendricks MR, So L, Green R, Roy CN, Sarkar SN, von Moltke J,

Anderson SK, Gale M, Savan R. 2019. Differential activation of the transcription factor IRF1 underlies the distinct immune responses elicited by type I and type III interferons. Immunity 51:451–464.e6. https://doi.org/10.1016/j.immuni.2019.07.007.
24. Mendoza JL, Schneider WM, Hoffmann H-H, Vercauteren K, Jude KM, Xiong A, Moraga I, Horton TM, Glenn JS, de Jong YP, Rice CM, Garcia KC. 2017. The IFN-λ-IFN-λR1-IL-10Rβ complex reveals structural features underlying type III IFN functional plasticity. Immunity 46:379–392. https://doi.org/10.1016/j.immuni.2017.02.017.
25. Galani IE, Triantafyllia V, Eleminiadou E-E, Koltsida O, Stavropoulos A, Manioudaki M, Thanos D, Doyle SE, Kotenko SV, Thanopoulou K, Andreakos E. 2017. Interferon-λ mediates non-redundant front-line antiviral protection against influenza virus infection without compromising host fitness. Immunity 46:875–890.e6. https://doi.org/10.1016/j.immuni.2017.04.025.
26. Davidson S, McCabe TM, Crotta S, Gad HH, Hessel EM, Beinke S, Hartmann R, Wack A. 2016. IFN λ is a potent anti-influenza therapeutic without the inflammatory side effects of IFN α treatment. EMBO Mol Med 8:1099–1112. https://doi.org/10.15252/emmm.201606413.
27. Broggi A, Tan Y, Granucci F, Zanoni I. 2017. IFN-λ suppresses intestinal inflammation by non-translational regulation of neutrophil function. Nat Immunol 18:1084–1093. https://doi.org/10.1038/ni.3821.
28. Saxena K, Simon LM, Zeng X-L, Blutt SE, Crawford SE, Sastri NP, Karandikar UC, Ajami NJ, Zachos NC, Kovbasnjuk O, Donowitz M, Conner ME, Shaw CA, Estes MK. 2017. A paradox of transcriptional and functional innate interferon responses of human intestinal enteroids to enteric virus infection. Proc Natl Acad Sci U S A 114:E570–E579. https://doi.org/10.1073/pnas.1615422114.
29. Pervolaraki K, Stanifer ML, Münchau S, Renn LA, Albrecht D, Kurzhals S, Senís E, Grimm D, Schröder-Braunstein J, Rabin RL, Boulant S. 2017. Type I and type III interferons display different dependency on mitogen-activated protein kinases to mount an antiviral state in the human gut. Front Immunol 8:459. https://doi.org/10.3389/fimmu.2017.00459.
30. Bhushal S, Wolfsmüller M, Selvakumar TA, Kemper L, Wirth D, Hornef MW, Hauser H, Köster M. 2017. Cell polarization and epigenetic status shape the heterogeneous response to type III interferons in intestinal epithelial cells. Front Immunol 8:671. https://doi.org/10.3389/fimmu.2017.00671.
31. Selvakumar TA, Bhushal S, Kalinke U, Wirth D, Hauser H, Köster M, Hornef MW. 2017. Identification of a predominantly interferon-λ-induced transcriptional profile in murine intestinal epithelial cells. Front Immunol 8:1302. https://doi.org/10.3389/fimmu.2017.01302.
32. Good C, Wells AI, Coyne CB. 2019. Type III interferon signaling restricts enterovirus 71 infection of goblet cells. Sci Adv 5:eaau4255. https://doi.org/10.1126/sciadv.aau4255.
33. Kolawole AO, Mirabelli C, Hill DR, Svoboda SA, Janowski AB, Passalacqua KD, Rodriguez BN, Dame MK, Freiden P, Berger RP, Vu D-L, Hosmillo M, O'Riordan MXD, Schultz-Cherry S, Guix S, Spence JR, Wang D, Wobus CE. 2019. Astrovirus replication in human intestinal enteroids reveals multicellular tropism and an intricate host innate immune landscape. PLoS Pathog 15:e1008057. https://doi.org/10.1371/journal.ppat.1008057.
34. Arimoto K-I, Miyauchi S, Stoner SA, Fan J-B, Zhang D-E. 2018. Negative regulation of type I IFN signaling. J Leukoc Biol 103:1099–1116. https://doi.org/10.1002/JLB.2MIR0817-342R.
35. Chen K, Liu J, Cao X. 2017. Regulation of type I interferon signaling in immunity and inflammation: a comprehensive review. J Autoimmun 83:1–11. https://doi.org/10.1016/j.jaut.2017.03.008.
36. Rothlin CV, Carrera-Silva EA, Bosurgi L, Ghosh S. 2015. TAM receptor signaling in immune homeostasis. Annu Rev Immunol 33:355–391. https://doi.org/10.1146/annurev-immunol-032414-112103.
37. Raudvere U, Kolberg L, Kuzmin I, Arak T, Adler P, Peterson H, Vilo J. 2019. g:Profiler: a Web server for functional enrichment analysis and conversions of gene lists (2019 update). Nucleic Acids Res 47:W191–W198. https://doi.org/10.1093/nar/gkz369.
38. Ashkenazi A, Dixit VM. 1999. Apoptosis control by death and decoy receptors. Curr Opin Cell Biol 11:255–260. https://doi.org/10.1016/s0955-0674(99)80034-9.
39. Heinz S, Benner C, Spann N, Bertolino E, Lin YC, Laslo P, Cheng JX, Murre C, Singh H, Glass CK. 2010. Simple combinations of lineage-determining transcription factors prime cis-regulatory elements required for macrophage and B cell identities. Mol Cell 38:576–589. https://doi.org/10.1016/j.molcel.2010.05.004.
40. Neil JA, Matsuzawa-Ishimoto Y, Kernbauer-Hölzl E, Schuster SL, Sota S, Venzon M, Dallari S, Galvao Neto A, Hine A, Hudesman D, Loke P, Nice TJ, Cadwell K. 2019. IFN-I and IL-22 mediate protective effects of intestinal viral infection. Nat Microbiol 4:1737–1749. https://doi.org/10.1038/s41564-019-0470-1.
41. Kernbauer E, Ding Y, Cadwell K. 2014. An enteric virus can replace the beneficial function of commensal bacteria. Nature 516:94–98. https://doi.org/10.1038/nature13960.
42. Miyoshi H, Stappenbeck TS. 2013. In vitro expansion and genetic modification of gastrointestinal stem cells in spheroid culture. Nat Protoc 8:2471–2482. https://doi.org/10.1038/nprot.2013.153.
43. Grabinger T, Luks L, Kostadinova F, Zimberlin C, Medema JP, Leist M, Brunner T. 2014. Ex vivo culture of intestinal crypt organoids as a model system for assessing cell death induction in intestinal epithelial cells and enteropathy. Cell Death Dis 5:e1228. https://doi.org/10.1038/cddis.2014.183.
44. Pott J, Kabat AM, Maloy KJ. 2018. Intestinal epithelial cell autophagy is required to protect against TNF-induced apoptosis during chronic colitis in mice. Cell Host Microbe 23:191–202.e4. https://doi.org/10.1016/j.chom.2017.12.017.
45. Nice TJ, Osborne LC, Tomov VT, Artis D, Wherry EJJ, Virgin HW. 2016. Type I interferon receptor deficiency in dendritic cells facilitates systemic murine norovirus persistence despite enhanced adaptive immunity. PLoS Pathog 12:e1005684. https://doi.org/10.1371/journal.ppat.1005684.
46. Dobin A, Davis CA, Schlesinger F, Drenkow J, Zaleski C, Jha S, Batut P, Chaisson M, Gingeras TR. 2013. STAR: ultrafast universal RNA-seq aligner. Bioinformatics 29:15–21. https://doi.org/10.1093/bioinformatics/bts635.
47. Wang L, Wang S, Li W. 2012. RSeQC: quality control of RNA-seq experiments. Bioinformatics 28:2184–2185. https://doi.org/10.1093/bioinformatics/bts356.
48. Ewels P, Magnusson M, Lundin S, Käller M. 2016. MultiQC: summarize analysis results for multiple tools and samples in a single report. Bioinformatics 32:3047–3048. https://doi.org/10.1093/bioinformatics/btw354.
49. Liao Y, Smyth GK, Shi W. 2014. featureCounts: an efficient general purpose program for assigning sequence reads to genomic features. Bioinformatics 30:923–930. https://doi.org/10.1093/bioinformatics/btt656.
50. Love MI, Huber W, Anders S. 2014. Moderated estimation of fold change and dispersion for RNA-seq data with DESeq2. Genome Biol 15:550. https://doi.org/10.1186/s13059-014-0550-8.
51. Neph S, Kuehn MS, Reynolds AP, Haugen E, Thurman RE, Johnson AK, Rynes E, Maurano MT, Vierstra J, Thomas S, Sandstrom R, Humbert R, Stamatoyannopoulos JA. 2012. BEDOPS: high-performance genomic feature operations. Bioinformatics 28:1919–1920. https://doi.org/10.1093/bioinformatics/bts277.
52. Platanitis E, Demiroz D, Schneller A, Fischer K, Capelle C, Hartl M, Gossenreiter T, Müller M, Novatchkova M, Decker T. 2019. A molecular switch from STAT2-IRF9 to ISGF3 underlies interferon-induced gene transcription. Nat Commun 10:2921. https://doi.org/10.1038/s41467-019-10970-y.